

Performance Evaluation of MIMO-FTN Signaling under Multipath Fading Channels with PA Non-linearity

Hao-Tse CHIU*, Shuhei SAITO*, Keita KURIYAMA†, Kentaro TANAKA†, Hitoshi HASEGAWA†, Toshifumi MIYAGI†, Takeshi ONIZAWA†, and Fumiaki MAEHARA*

*Graduate School of Fundamental Science and Engineering, Waseda University,
3-4-1 Ohkubo, Shinjuku-ku, Tokyo 169-8555, Japan

†NTT Access Network Service Systems Laboratories, Nippon Telegraph and Telephone Corporation,
1-1 Hikarino-oka, Yokosuka-shi, Kanagawa 239-0847, Japan

Email: *fumiaki_m@waseda.jp

Abstract—In this study, we investigate the system performance of multiple-input multiple-output (MIMO) faster-than-Nyquist (FTN) signaling in the context of power amplifier (PA) non-linearity under multipath fading channels. We apply a more general MIMO-FTN precoded orthogonal frequency division multiplexing (OFDM) system model and provide the corresponding input-output relationship. For the PA model, the Rapp model is adopted to characterize the effect of non-linear distortion. We intend to investigate system performance through simulations under the following conditions: employing the MIMO configuration, utilizing the FTN signaling scheme, operating in a multipath environment, and accounting for PA non-linearity. This aspect has received relatively limited attention thus far. The simulation results reveal that FTN signaling still performs better than Nyquist signaling under the fixed transmission rate. For more comprehensive research, the effects of PA non-linearity are also simply demonstrated.

Index Terms—Faster-than-Nyquist (FTN) signaling, multiple-input multiple-output (MIMO), power amplifier (PA) non-linearity, colored noise, multipath channel.

I. INTRODUCTION

Recently, the standards for sixth-generation wireless communication (6G) are in ongoing discussion and envisioned to support Tbps-level peak data rates to fulfill the exponentially increasing traffic demand for mobile broadband services [1], [2]. Generally, conventional wireless communication systems frequently adopt the Nyquist criterion in the system design to achieve inter-symbol interference (ISI)-free transmission. Under the Nyquist criterion, the symbol period is lower-bounded by a specific value T_0 , which is the reciprocal of the system bandwidth. To break the limitation and achieve higher data rates and spectral efficiency, a concept called faster-than-Nyquist (FTN) signaling has gradually come into researchers' view since the 1970s [3]–[6].

In FTN signaling, the symbol period of the data transmission is chosen as a compressed one of $T = \zeta T_0$, where ζ represents the compression factor (or symbol packing ratio) in the time domain. By relaxing the orthogonality characteristics and allowing ISI intentionally, the data rate is expected to be improved without the bandwidth expansion compared to

Nyquist signaling [3], [4]. However, in exchange for the transmission rate, ISI will lead to performance degradation in the FTN systems.

Aside from squeezing the transmitted data, applying multiple antennas at the transceiver side is another well-known method to realize a higher transmission rate effectively. Consequently, over the past few decades, FTN signaling under multiple-input multiple-output (MIMO) configuration has attracted significant attention [7]–[11]. First, the Mazo limit of a MIMO channel was investigated in [7]. The authors in [8] proposed a MIMO-FTN-single carrier (SC) signaling method and a low-cost decision feedback and frequency domain equalization (FDE) algorithm. The authors in [9] considered the MIMO-FTN systems employing SC-FDE, where the equalization matrices included the impact of colored noise and were approximated to reduce the computational complexity. In [10], [11], capacity expressions for MIMO-FTN-SC systems under frequency flat and frequency selective channels were derived and the superiority of the MIMO technique was also verified.

As mentioned previously, ISI induced by FTN signaling is inevitable, which will also influence the peak-to-average-power ratio (PAPR) of the transmitted signal. Meanwhile, when the signal is transmitted in practical systems, higher PAPR might probably suffer from amplitude distortion owing to the nonlinear region of power amplifiers (PA), which was not considered in the above MIMO works. In [12], the impact of non-linearities was shown and FTN signaling was regarded as a promising solution to reduce the PAPR under a constant transmission rate by utilizing lower-order modulation schemes. Based on the aforementioned pioneering work, the authors in [13] investigated the performance of single-input single-output (SISO)-FTN signaling considering PA non-linearity under multipath fading channels.

Distinct from the above literature, this work extends the current research to MIMO schemes and studies the performance evaluations of FTN signaling in the presence of PA non-linearity. We adopt a more general MIMO-FTN system

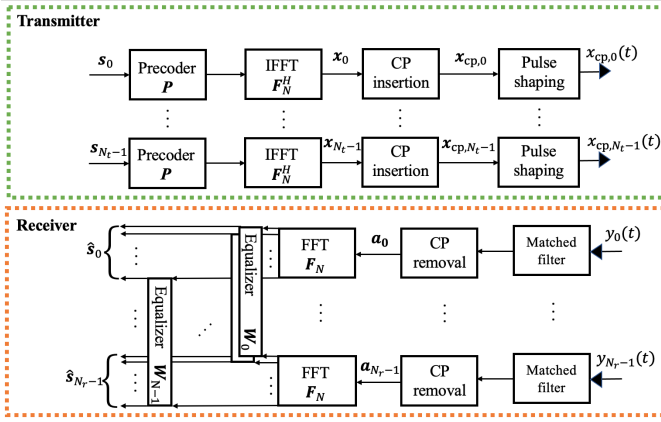


Fig. 1: The MIMO-FTN signaling system block diagram.

to support the most widely-used waveforms like SC-FDE. To characterize the PA non-linearity, the Rapp model [14], [15] is used in our computer simulations. With such imperfection, the performance comparisons between FTN and Nyquist signaling are revealed assuming the same-bit transmission, which clarifies the effectiveness of MIMO-FTN signaling under multipath fading channels.

The rest of the paper is organized as follows. Section II introduces a MIMO system utilizing FTN signaling, followed by the mathematical analysis including spatial and spectral precoding, and the expressions of equalizers considering the colored noise are introduced. Simulation results reveal the advantages of MIMO-FTN signaling in terms of bit error rate (BER) and normalized throughput under multipath fading channels and PA non-linearity in Section III. Finally, this study concludes in Section IV.

II. SYSTEM MODEL

First, we introduce a more general MIMO-FTN system model in this study. The transceiver block diagram of a MIMO-FTN-SCFDE can be schematized in Fig. 1. The transmitter and the receiver are equipped with N_t and N_r antennas, respectively. For the p -th data stream ($0 \leq p \leq N_t - 1$), an N -length complex-valued symbol vector $\mathbf{s}_p = [s_{p,0}, \dots, s_{p,N-1}]^T \in \mathbb{C}^N$ with zero mean and unit variance is transmitted. At the transmitter, each symbol vector is multiplied by a precoding matrix \mathbf{P} followed by an N -point inverse discrete Fourier transform (IDFT) matrix \mathbf{F}_N^H , whose (m, n) -th entry is $e^{j2\pi mn/N}/\sqrt{N}$. Next, a G -length cyclic prefix (CP) is inserted in front of the information-bearing signal \mathbf{x}_p to avoid inter-block interference (IBI):

$$\mathbf{x}_{cp,p} = \mathbf{A}_{cp} \mathbf{F}_N^H \mathbf{P} \mathbf{s}_p, \quad \mathbf{A}_{cp} = \begin{bmatrix} \mathbf{0}_{G \times (N-G)} & \mathbf{I}_G \\ & \mathbf{I}_N \end{bmatrix}. \quad (1)$$

After the CP insertion, a pulse-shaping filter $g(t)$ is applied to the CP-inserted signal $\mathbf{x}_{cp,p}$ of length $N + G$ with n -th entry $[\mathbf{x}_{cp,p}]_n$ in the time domain. Throughout this study, we assume $g(t)$ is a root-raised cosine (RRC) filter with a roll-off factor α and unit energy [16]. To realize the FTN transmission, the

symbol is sampled by the interval T to generate the pulse-shaped FTN signal:

$$x_{cp,p}(t) = \sum_{n=0}^{N+G-1} [\mathbf{x}_{cp,p}]_n g(t - nT), \quad T = \zeta T_0, \quad (2)$$

where T_0 is the minimum symbol interval under the Nyquist criterion, and ζ , $0 < \zeta \leq 1$ represents the compression/squeezing factor in the time domain. We assume each pulse-shaped FTN signal stream is sent over a frequency-selective channel with channel order L $\mathbf{h}_{q,p} \in \mathbb{C}^L$ between the p -th transmit antenna and the q -th receive antenna ($0 \leq q \leq N_r - 1$), where the channel coefficients are denoted by $[\mathbf{h}_{q,p}]_l$ ($l = 0, 1, \dots, L - 1$).

At the receiver, a matched filter $g^*(-t)$ is adopted to maximize the received signal-to-noise ratio (SNR) [17], [18], and the resultant signals are also sampled at interval T . Therefore, the filtered signal of the q -th receive branch $y_q(t)$ can be represented as [9]

$$y_q(t) = \sum_{p=0}^{N_t-1} \sum_{l=0}^{L-1} \sum_n [\mathbf{h}_{q,p}]_l [\mathbf{x}_{cp,p}]_n \gamma(t - (l+n)T) + \eta_q(t), \quad (3)$$

where

$$\gamma(t) = \int_{-\infty}^{\infty} g(\xi) g^*(t - \xi) d\xi, \quad \eta_q(t) = \int_{-\infty}^{\infty} n_q(\xi) g^*(t - \xi) d\xi, \quad (4)$$

and $n_q(t)$ represents a complex additive white Gaussian noise (AWGN) of q -th receive antenna with variance N_0 . Then, the CP removal is performed, and the N -length received time-domain signal $\mathbf{a} \in \mathbb{C}^N$ can be obtained as

$$\mathbf{a}_q = \sum_{p=0}^{N_t-1} \mathbf{R}_{cp} \mathbf{H}_{\text{ISI},q,p} \mathbf{x}_{cp,p} + \boldsymbol{\eta}_q, \quad (5)$$

$$\mathbf{R}_{cp} = \begin{bmatrix} \mathbf{0}_{N \times \frac{G}{2}} & \mathbf{I}_N & \mathbf{0}_{N \times \frac{G}{2}} \end{bmatrix},$$

where \mathbf{R}_{cp} denotes the CP removal matrix, $\mathbf{H}_{\text{ISI},q,p} \in \mathbb{C}^{(N+G) \times (N+G)}$ describes the channel matrix including the effects of ISI induced by FTN signaling and the multipath fading, and $\boldsymbol{\eta}_q$ is the sampled version of $\eta_q(t)$. Specifically, the (k, m) -th entries of $\mathbf{H}_{\text{ISI},q,p}$ can be calculated by

$$[\mathbf{H}_{\text{ISI},q,p}]_{k,m} = \sum_{l=0}^{L-1} [\mathbf{h}_{q,p}]_l \gamma(kT - (m+l)T). \quad (6)$$

Moreover, in this study, we assume the CP length is sufficiently long as $G > 2L$ and $g(kT) = 0$, $|k| > \frac{G}{2}$. Under these assumptions, the approximated channel matrix $\mathbf{H}_{q,p,\text{approx}} = \mathbf{R}_{cp} \mathbf{H}_{q,p,\text{ISI}} \mathbf{A}_{cp}$ will become circulant, and the input-output relationship is given by [18]

$$\mathbf{a}_q \approx \sum_{p=0}^{N_t-1} \mathbf{H}_{q,p,\text{approx}} \mathbf{x}_p + \boldsymbol{\eta}_q. \quad (7)$$

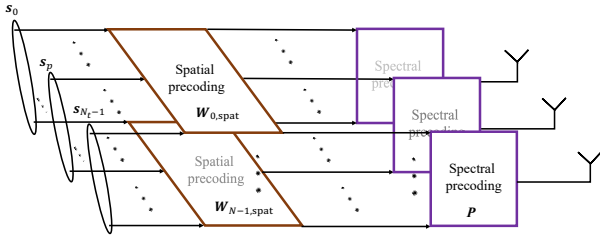


Fig. 2: Illustration of the spatial and spectral precoding.

where \mathbf{x}_p denotes the signal vector of p -th transmit antenna after CP insertion. Based on the circularity above, $\mathbf{H}_{q,p,\text{approx}}$ can be diagonalized by the DFT matrices $\mathbf{H}_{q,p,\text{approx}} = \mathbf{F}_N^H \mathbf{A}_{q,p} \mathbf{F}_N$. When G is not long enough, $\mathbf{H}_{q,p,\text{approx}}$ will no longer be circulant. In such a condition, the off-diagonal terms in $\mathbf{A}_{q,p}$ appear and will consequently be detrimental to the detection performance.

Subsequently, we turn to analyze the overall input-output relationship based on the MIMO systems. The precoding procedures of a MIMO system can be divided into spectral and spatial modulation [19] as Fig. 2 shows, corresponding to the frequency and spatial domain, respectively. With the derivation given in [19, Lemma 1], an overall effective channel matrix \mathbf{H}_{eff} can be defined:

$$\mathbf{H}_{\text{eff}} = \mathbf{W}_{\text{spec}} \circ (\mathbf{H} \mathbf{W}_{\text{spat}}) \quad (8)$$

where $\mathbf{W}_{\text{spec}} \in \mathbb{C}^{N_r N \times N_t N}$ represents the extended spectral precoding matrix calculated by \mathbf{P} in (1), \circ symbolizes the Hadamard product, $\mathbf{H} \in \mathbb{C}^{N_r N \times N_t}$ collects MIMO channel coefficients, and $\mathbf{W}_{\text{spat}} \in \mathbb{C}^{N_t \times N_t N}$ concatenates the spatial precoded matrices on the subcarrier level, *i.e.*, $\mathbf{W}_{\text{spat}} = [\mathbf{W}_{0,\text{spat}}, \dots, \mathbf{W}_{N-1,\text{spat}}]$. To simplify the analysis, we choose the case with $\mathbf{W}_{n,\text{spat}} = \mathbf{I}_{N_t}$, $n = 0, \dots, N-1$ in this study, and the comparisons between different spatial precoders will be left for future work.

On the other hand, because each coefficient of the precoding matrix \mathbf{P} will affect all the $N_r \times N_t$ MIMO channel matrices equivalently for each subcarrier, the spectral precoding matrix \mathbf{W}_{spec} is obtained by

$$\mathbf{W}_{\text{spec}} = \mathbf{P} \otimes \mathbf{1}_{N_r, N_t} \quad (9)$$

where \otimes denotes the Kronecker product and $\mathbf{1}_{N_r, N_t}$ denotes an all-ones matrix with size $N_r \times N_t$.

Finally, for the collection of MIMO channels \mathbf{H} , it is acquired by rearranging the diagonal matrices $\mathbf{A}_{q,p}$ based on the subcarrier index as

$$\mathbf{H}_n = \begin{bmatrix} [\mathbf{A}_{0,0}]_{n,n} & \cdots & [\mathbf{A}_{0,N_t-1}]_{n,n} \\ \vdots & \ddots & \vdots \\ [\mathbf{A}_{N_r-1,0}]_{n,n} & \cdots & [\mathbf{A}_{N_r-1,N_t-1}]_{n,n} \end{bmatrix} \in \mathbb{C}^{N_r \times N_t} \quad (10)$$

and channels per-subcarrier \mathbf{H}_n further comprise $\mathbf{H} = [\mathbf{H}_0^T, \dots, \mathbf{H}_{N-1}^T]^T$. Next, we also need to rearrange other related vectors in a similar way. Here, we define the overall input

data vector as $\mathbf{t} = [\mathbf{t}_0^T \cdots, \mathbf{t}_n^T \cdots, \mathbf{t}_{N-1}^T]^T \in \mathbb{C}^{N_t N}$, $\mathbf{t}_n = [s_{n,0}, \dots, s_{n,N_t-1}]^T$, and the received signal \mathbf{a}_q , noise vector $\boldsymbol{\eta}_q$ in (7) as $\mathbf{r}, \boldsymbol{\eta}$. The overall transmission from \mathbf{t} to \mathbf{r} can be expressed as a single MIMO transmission:

$$\mathbf{r} = \mathbf{H}_{\text{eff}} \mathbf{t} + \boldsymbol{\eta}. \quad (11)$$

After clarifying the input-output relationship, the next step is signal recovery by frequency domain equalization (FDE). An N -point DFT converts the received signal of each antenna to the frequency domain followed by a FDE matrix in the minimum mean square error (MMSE) sense, which is mathematically equivalent to [6], [20]:

$$\mathbf{W}_{\text{MMSE}} = \mathbf{H}_{\text{eff}}^H (\mathbf{H}_{\text{eff}} \mathbf{H}_{\text{eff}}^H + \frac{1}{E_s} (\mathbf{F}_N^H \otimes \mathbf{I}_{N_r}) \mathbb{E}[\boldsymbol{\eta} \boldsymbol{\eta}^H] (\mathbf{F}_N \otimes \mathbf{I}_{N_r}))^{-1}. \quad (12)$$

where E_s represents the power of the transmitted signal. However, because the sampling rate at the receiver is set to be faster than the Nyquist rate, the noise at each receive antenna $\boldsymbol{\eta}_q$ would become colored noise, whose corresponding covariance matrices are computed by

$$\begin{aligned} \mathbb{E}[\boldsymbol{\eta}_q \boldsymbol{\eta}_q^H] &= N_0 \boldsymbol{\Gamma} \in \mathbb{R}^{N \times N}, \\ [\boldsymbol{\Gamma}]_{k,m} &= \gamma((k-m)T). \end{aligned} \quad (13)$$

If the covariance matrix is far from diagonal, the term $\mathbb{E}[\boldsymbol{\eta} \boldsymbol{\eta}^H]$ will break the subcarrier-wise calculation and lead to high computation complexity when one computes the inverse operation in (12). Thus, to maintain the diagonality of $\mathbb{E}[\boldsymbol{\eta} \boldsymbol{\eta}^H]$, [6] proposed that the noise-related term $\mathbf{F}_N^H \mathbb{E}[\boldsymbol{\eta}_q \boldsymbol{\eta}_q^H] \mathbf{F}_N$ in (13) can be approximated by a diagonal matrix $N_0 \boldsymbol{\Phi}_q$ to reduce the computation loading, whose n -th diagonal entry is

$$[\boldsymbol{\Phi}_q]_n = \frac{1}{N} \sum_{k=0}^{N-1} \sum_{m=0}^{N-1} g((k-m)T) e^{j2\pi \frac{(k-m)n}{N}}. \quad (14)$$

Finally, we can linearly obtain the time-domain estimated data vector $\hat{\mathbf{t}}$ by $\hat{\mathbf{t}} = \mathbf{W}_{\text{MMSE}} (\mathbf{F}_N \otimes \mathbf{I}_{N_r}) \mathbf{r}$.

III. SIMULATION RESULT

Computer simulations by MATLAB are performed in this section to demonstrate the effectiveness of MIMO configuration with FTN signaling and compare the performance difference between SC-FDE ($\mathbf{P} = \mathbf{F}_N$) and OFDM ($\mathbf{P} = \mathbf{I}_N$) systems under multipath fading channels and PA non-linearity. The data block, CP, and channel lengths are set to be $N = 128$, $G = 30$, and $L = 30$, respectively. The constellation pattern for 16APSK with unit average power is [4, 12], of which 4 inner points are concentric with inner/outer radius ratio = 2.57. Moreover, we assign the channel coefficients $[\mathbf{h}]_l$ of an L -tap fading channel with the distribution $\mathcal{CN}(0, 1/L)$ and assume the channel estimation is ideal. To acquire more accurate results, at least 5000 Monte Carlo trials are conducted for each parameter setting.

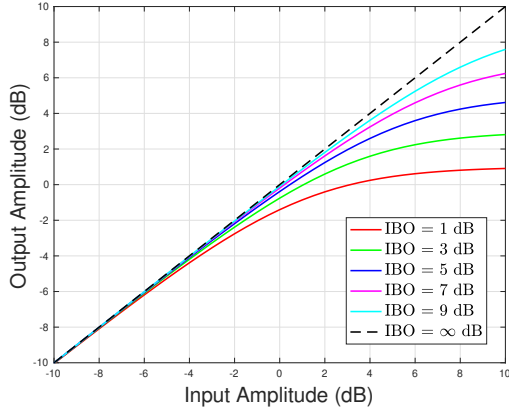
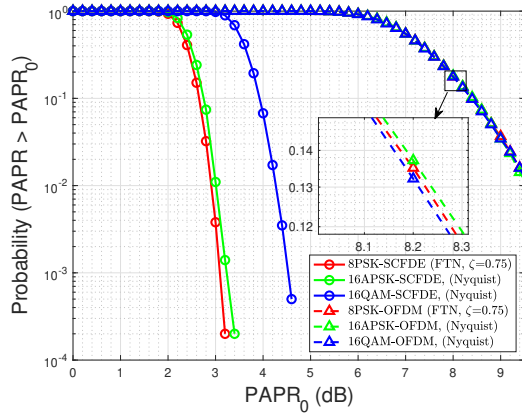


Fig. 3: The input/output relationship of the Rapp model.

Fig. 4: PAPR performance of systems with $\alpha = 0.5$ employing 8PSK ($\zeta = 0.75$), 16QAM (Nyquist), and 16APSK (Nyquist) before the PA.

To describe the effect of PA non-linearity, the Rapp model is adopted. The input-output relationship of a PA employing the Rapp model can be expressed as [14], [15]

$$A_{\text{out}}(t) = \frac{\nu A_{\text{in}}(t)}{[1 + (\frac{A_{\text{in}}(t)}{A_{\text{sat}}})^{2\rho}]^{\frac{1}{2\rho}}}, \quad (15)$$

where ν is the small signal gain, $A_{\text{in}}(t)$ and $A_{\text{out}}(t)$ are the amplitudes of input and output signals, respectively, and A_{sat} is the saturation amplitude determined by the input back-off (IBO) $\xi = |A_{\text{sat}}|^2 / \mathbb{E}\{|y_q(t)|^2\}$. When $\xi \rightarrow \infty$, the PA non-linearity will be absent, and (15) becomes a linear operation (*i.e.*, ideal PA). The effect of the Rapp model on the input/output amplitudes of a PA is simply depicted in Fig. 3. Herein, the nonlinear factor ρ is chosen as 0.81 [15] and without loss of generality, ν is set to be 1.

First, the PAPR performance before the PA is shown in Fig. 4. In the simulation, the compressing factors are chosen based on the criterion of same-bit transmission. For example, the 4-bit transmission considered in Fig. 4 corresponds to Nyquist-16APSK, Nyquist-16QAM, and FTN-8PSK with $\zeta = 0.75$ decided by the factor $(\log_2 M)/\zeta$. It can be found that for pulse-shaping SC-FDE systems, FTN-8PSK is slightly better than

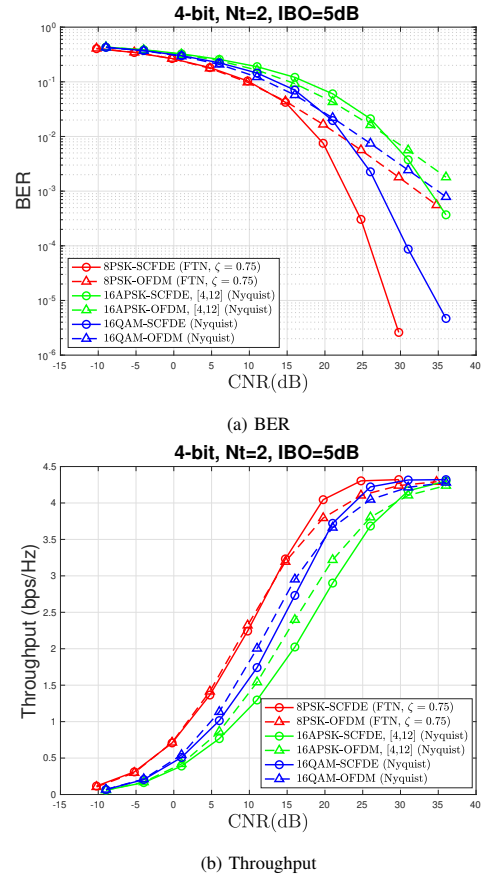
Nyquist-16APSK/16QAM due to the symbol compression of FTN, which allows a lower level of modulation scheme, but all of them still outperform OFDM cases as expected.

Hereafter, signals go through the Rapp model and experience the potential distortion. For the value of IBO, [15] suggests 0.5dB for SC-FDE and 8dB for OFDM. To take a balanced value for the comparisons, we consider $\xi = 5$ dB for PA non-linearity unless otherwise specified. Besides, in this study, system throughput is also selected as one of the performance metrics. To calculate the system throughput, we approximate it by a binary entropy function $H(x) = -x \log_2 x - (1-x) \log_2 (1-x)$, which is given by [6], [9], [21]

$$\text{Throughput} = \frac{N}{N+G} \sum_{p=0}^{N_t-1} \frac{\log_2 M}{\zeta(1+\alpha)} (1 - H(P_{e,p})) \quad (16)$$

where M and $P_{e,p}$ denote the constellation size of the modulation scheme and the bit error rate (BER) of the p -th stream obtained by the numerical simulations, respectively.

Next, we reveal both BER and throughput performance when $\alpha = 0.5$ and $N_t = N_r = 2$. In every case, the carrier-to-noise ratio (CNR) is defined as $\text{CNR} = E_b/N_0 \times \log_2 M$ (dB), where E_b represents the energy per bit. In Fig. 5, one can

Fig. 5: Performance comparisons between 2×2 MIMO-FTN and Nyquist signaling under 4-bit transmission with $\xi = 5$ dB.

observe that FTN signaling accompanies better performance than conventional Nyquist signaling. This is also because the modulation scheme of lower order is utilized when the symbol period is compressed but the transmission rate is still retained. In both FTN and Nyquist signaling, SC-FDE outperforms OFDM from approximately $\text{CNR} = 15$ dB ($M = 8$) and $\text{CNR} = 20$ dB ($M = 16$), which results from better frequency diversity exploited by MMSE-SCFDE [22, Chap. 6, 7].

Finally, in Fig. 6, we provide a comparison including the impact of PA non-linearity on the BER performance. As expected, performance degradation appears when IBO is introduced and becomes more severe with decreasing ξ . This phenomenon originates from the fact that the distorted signals might invoke probable detection errors. FTN-8PSK has better asymptotic performance than others because the distortion induced by PA non-linearity has less influence on the signal employing a lower level of modulation scheme, which has a larger minimum Euclidean distance (MED). Moreover, it can be seen that increasing IBO leads to less improvement for OFDM cases because of the inter-carrier interference (ICI) caused by signal compression.

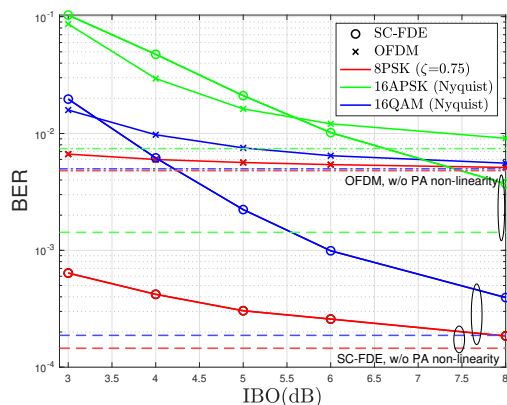


Fig. 6: BER performance of 2×2 MIMO-FTN signaling under 4-bit transmission with and without PA non-linearity when $E_b/N_0 = 20$ dB.

IV. CONCLUSION

In this study, the performance of MIMO-FTN systems in the context of PA non-linearity was investigated. We introduced a MIMO-FTN system model and included SC-FDE and OFDM systems for the comparisons, where spatial and spectral precoding procedures formulated the overall modulation. To reveal the effectiveness of FTN signaling, we focus on fixed-bit transmission with higher-level modulation schemes. Simulation results demonstrated the effectiveness of FTN signaling in 4-bit transmission. Besides, we verified the performance degradation resulting from PA non-linearity by modulating the value of IBO, where the error floor is higher for OFDM cases because they suffer from ICI and lack of frequency diversity.

ACKNOWLEDGMENT

The authors would like to thank Dr. H. Suganuma for his continuing support.

REFERENCES

- [1] Z. Zhang, Y. Xiao, Z. Ma, M. Xiao, Z. Ding, X. Lei, G. K. Karagiannidis, and P. Fan, "6G wireless networks: Vision, requirements, architecture, and key technologies," *IEEE Vehicular Technology Magazine*, vol. 14, no. 3, pp. 28–41, 2019.
- [2] "White paper - 5G evolution and 6G," Japan, NTT Docomo Inc., White Paper, Jan. 2022.
- [3] J. E. Mazo, "Faster-than-Nyquist signaling," *The Bell System Technical Journal*, vol. 54, no. 8, pp. 1451–1462, Oct. 1975.
- [4] J. B. Anderson, F. Rusek, and V. Öwall, "Faster-than-Nyquist signaling," *Proceedings of the IEEE*, vol. 101, no. 8, pp. 1817–1830, Aug. 2013.
- [5] J. Fan, S. Guo, X. Zhou, Y. Ren, G. Y. Li, and X. Chen, "Faster-than-Nyquist signaling: An overview," *IEEE Access*, vol. 5, pp. 1925–1940, Feb. 2017.
- [6] T. Ishihara, S. Sugiura, and L. Hanzo, "The evolution of faster-than-Nyquist signaling," *IEEE Access*, vol. 9, pp. 86 535–86 564, June 2021.
- [7] F. Rusek, "On the existence of the Mazo-limit on MIMO channels," *IEEE Transactions on Wireless Communications*, vol. 8, no. 3, pp. 1118–1121, 2009.
- [8] M. McGuire, A. Dimopoulos, and M. Sima, "Faster-than-Nyquist single-carrier MIMO signaling," in *2016 IEEE Globecom Workshops (GC Wkshps)*, 2016, pp. 1–7.
- [9] Y. Kumagai, A. Nakamura, S. Saito, H. Suganuma, K. Kuriyama, Y. Ono, H. Fukuzono, M. Yoshioka, and F. Maehara, "Performance improvement of faster-than-Nyquist single-carrier MIMO signaling considering the effects of colored noise," *IEICE Communications Express*, vol. 11, no. 4, pp. 176–182, Apr. 2022.
- [10] M. Yuhas, Y. Feng, and J. Bajcsy, "On the capacity of faster-than-Nyquist MIMO transmission with CSI at the receiver," in *2015 IEEE Globecom Workshops (GC Wkshps)*, 2015, pp. 1–6.
- [11] Z. Zhang, M. Yuksel, and H. Yanikomeroğlu, "Faster-than-Nyquist signaling for MIMO communications," *IEEE Transactions on Wireless Communications*, vol. 22, no. 4, pp. 2379–2392, 2023.
- [12] J.-A. Lucciardi, N. Thomas, M.-L. Boucheret, C. Poulliat, and G. Mesnager, "Trade-off between spectral efficiency increase and PAPR reduction when using FTN signaling: Impact of non linearities," in *2016 IEEE International Conference on Communications (ICC)*, 2016, pp. 1–7.
- [13] A. Nakamura, Y. Kumagai, S. Saito, H. Suganuma, K. Kuriyama, Y. Ono, H. Fukuzono, M. Yoshioka, and F. Maehara, "Effectiveness evaluation of FTN signaling in the presence of nonlinear distortion under multipath fading channels," *IEICE Communications Express*, vol. 11, no. 2, pp. 104–110, 2022.
- [14] C. Rapp, "Effects of HPA-nonlinearity on 4-DPSK/OFDM-signal for a digital sound broadcasting system," in *2nd European Conference on Satellite Communication*, Oct. 1991, pp. 179–184.
- [15] L. Cariou and G. Venkatesan, "TGay evaluation methodologs," *IEEE 802.11-15/0866r2*, Jan. 2016.
- [16] J. Anderson and A. Svensson, *Coded Modulation Systems*. Springer, 2003.
- [17] S. Haykin, *Communication Systems, 4th edition*. New York: Wiley, 2001.
- [18] T. Ishihara and S. Sugiura, "Reduced-complexity FFT-spread multicarrier faster-than-Nyquist signaling in frequency-selective fading channel," *IEEE Open Journal of the Communications Society*, vol. 3, pp. 530–542, Mar. 2022.
- [19] R.-A. Pitaval and B. M. Popović, "Linear receivers for spectrally-precoded MIMO-OFDM," *IEEE Communications Letters*, vol. 21, no. 6, pp. 1269–1272, 2017.
- [20] H. Fukumoto and K. Hayashi, "Overlap frequency domain equalization for faster-than-Nyquist signaling," Sept. 2015. [Online]. Available: <https://arxiv.org/abs/1509.00562>
- [21] K. Kojima, Y. Shimbo, H. Suganuma, and F. Maehara, "Deep learning based CoMP transmission method using vehicle position information for taxi radio systems," in *2020 International Conference on Artificial Intelligence in Information and Communication (ICAIC)*, 2020, pp. 253–256.
- [22] Y.-P. Lin, S.-M. Phoong, and P. P. Vaidyanathan, *Filter Bank Transceivers for OFDM and DMT Systems*. Cambridge, U.K.: Cambridge Univ. Press, 2011.